

Dalton Transactions

Accepted Manuscript



This is an *Accepted Manuscript*, which has been through the Royal Society of Chemistry peer review process and has been accepted for publication.

Accepted Manuscripts are published online shortly after acceptance, before technical editing, formatting and proof reading. Using this free service, authors can make their results available to the community, in citable form, before we publish the edited article. We will replace this *Accepted Manuscript* with the edited and formatted *Advance Article* as soon as it is available.

You can find more information about *Accepted Manuscripts* in the [Information for Authors](#).

Please note that technical editing may introduce minor changes to the text and/or graphics, which may alter content. The journal's standard [Terms & Conditions](#) and the [Ethical guidelines](#) still apply. In no event shall the Royal Society of Chemistry be held responsible for any errors or omissions in this *Accepted Manuscript* or any consequences arising from the use of any information it contains.

Cite this: DOI: 10.1039/c0xx00000x

www.rsc.org/xxxxxx

ARTICLE TYPE

Aqueous citrato-oxovanadate(IV) precursor solutions for VO₂: synthesis, spectroscopic investigation and thermal analysis

Nick Peys,^{a,b} Peter Adriaensens,^c Sabine Van Doorslaer,^d Sven Gielis,^{a,e} Ellen Peeters,^a Christopher De Dobbelaere,^a Stefan De Gendt,^{b,f} An Hardy,^{a,e} and Marlies K. Van Bael,^{*a,e}

Received (in XXX, XXX) Xth XXXXXXXXX 20XX, Accepted Xth XXXXXXXXX 20XX

DOI: 10.1039/b000000x

An aqueous precursor solution, containing citrato-VO²⁺ complexes, is synthesized for the formation of monoclinic VO₂. With regard to the decomposition of the VO²⁺ complexes towards vanadium oxide formation, it is important to gain insights in the chemical structure and transformations of the precursor during synthesis and thermal treatment. Hence, the conversion of the cyclic [V₄O₁₂]⁴⁻ ion to the VO²⁺ ion in the aqueous solution, using oxalic acid as acidifier and reducing agent, is studied by ⁵¹Vanadium Nuclear Magnetic Resonance spectroscopy. The citrate complexation of this VO²⁺ ion and the differentiation between a solution containing citrato-oxalato-VO²⁺ and citrato-VO²⁺ complexes is studied by Electron Paramagnetic Resonance and Fourier Transform Infra-Red spectroscopy. In both solutions, the VO²⁺ containing complex is mononuclear and has a distorted octahedral geometry with a fourfold R-CO₂⁻ ligation at the equatorial positions and likely a fifth R-CO₂⁻ ligation at the axial position. Small differences in the thermal decomposition pathway between the gel containing citrato-oxalato-VO²⁺ complexes and the oxalate-free gel containing citrato-VO²⁺ complexes are observed between 150 and 200 °C in air and are assigned to the presence of (NH₄)₂C₂O₄ in the citrato-oxalato-VO²⁺ solution. Both precursor solutions are successfully used for the formation of crystalline vanadium oxide nanostructures on SiO₂, after a thermal anneal at 500 °C in a 0.1 % O₂ ambient. However, the citrato-oxalato-VO²⁺ and the oxalate-free citrato-VO²⁺ solution result in the formation of monoclinic V₆O₁₃ and monoclinic VO₂, respectively.

Introduction

Vanadium exists in different oxidation states, ranging from +II to +V, forming a variety of vanadium oxides. This variety includes single valence oxides (such as V₂O₃, VO₂ and V₂O₅) and mixed valence oxides (such as V₆O₁₃ and V₃O₇).^{1,2} Some of these vanadium oxides with a specific structure and crystallinity are intensively investigated as candidate active materials in future technological devices. (i) Monoclinic VO₂ M1 exhibits a temperature induced semiconductor-to-metal transition at a temperature of 68 °C. This transition is accompanied by a structural, monoclinic to tetragonal, phase transition with a lattice distortion along the c-axis. During the transition, its electrical resistivity and infrared optical properties abruptly changes.³⁻⁵ The change in electrical resistivity and infrared transmittance is associated with a hysteresis loop around 68 °C. In bulk materials and thin films, this hysteresis width is about 1 °C and 10-15 °C, respectively.⁵ However, in VO₂ particles a larger hysteresis width in the order of 30 °C has been observed.^{6,7} This makes them more applicable as a switching material in memory and optical devices.⁵ For its synthesis, caution is required, because up to six

polymorphs have been reported for VO₂. These polymorphs include VO₂ B and VO₂ M1 which belong to the monoclinic space groups C2/m and P2₁/c, respectively.⁵ (ii) Layered vanadium oxides, such as V₆O₁₃, are proposed as alternatives for the reasonably thermally unstable and expensive LiCoO₂ cathode in rechargeable Li-ion micro-batteries.^{8,9} V₆O₁₃ single crystals exhibit a lithium intercalation/extraction plateau around 2.7 V vs. a Li/Li⁺ reference electrode and reversibly host up to 6 Li atoms per formula unit, leading to a maximal theoretical gravimetric charge capacity of 310 mAhg⁻¹.^{10,11}

As evidenced by the large variety of vanadium oxides and the complex vanadium-oxygen phase diagram¹, the synthesis of VO₂ is not straightforward. In addition, the occurrence of multiple VO₂ polymorphs further emphasises the challenge to synthesize stoichiometric and phase pure monoclinic VO₂. Various methods for the synthesis of VO₂ have been reported including chemical vapour deposition^{5,12}, atomic layer deposition^{13,14}, pulsed laser deposition^{5,15} and sputtering^{5,16,17}. Wet chemical synthesis routes are widely considered as valuable alternatives for the vacuum based techniques.¹⁸ In these routes, VO₂ is commonly prepared starting from vanadium alkoxides.^{5,19,20} However, such alkoxides are scarcely available, expensive and very reactive to ambient

humidity.¹⁸ Alternatively, aqueous synthesis routes are proposed by Livage et al. and Dachaun et al. who prepared VO₂ films starting from a V₂O₅ gel or sol, respectively.^{21,22} However, the aforementioned wet chemical routes intermediately form V₂O₅ films and require an additional, reductive anneal to obtain VO₂ films.^{21,22} This emphasizes the large challenge in the direct formation of VO₂ M1 from an aqueous solution.

In a previous study, we reported the synthesis of an aqueous VO²⁺ precursor solution for the formation of V₆O₁₃ on Al₂O₃. The emphasis was on the thermal conversion of the deposited precursor solution to the desired oxide phase. The main parameters of this thermal step including pO₂, temperature and time were investigated.²³ However, in the present study, we aim at the direct formation of monoclinic VO₂, without the intermediate V₂O₅ phase, from an aqueous precursor solution containing citrato-oxovanadate(IV) complexes. A strong emphasis lies on the fundamental understanding of the pH dependent behaviour of the vanadium(V) and vanadium(IV) ion in an aqueous solution and its citrate complexation. Additionally, to understand the conversion of the VO²⁺ complexes to the solid vanadium oxides, it is crucial to gain insights in the chemical transformations during thermal treatment. Finally, the precursor solution is successfully used for the formation of crystalline VO₂ M1 nanostructures on SiO₂. This fundamental study contributes to a better understanding of the aqueous VO²⁺ chemistry in the presence of citrate compounds and proposes an entirely water-based method for the direct formation of crystalline VO₂ M1.

Experimental

Synthesis of the aqueous solutions

The synthesis of the aqueous citrato-oxalato-oxovanadate(IV) and the oxalate free citrato-oxovanadate(IV) precursor solutions is schematically given in Figure 1. Initially, an aqueous VO²⁺ solution was synthesized as described earlier.²³ In this synthesis, ammonium metavanadate (NH₄VO₃, ≥99 %, Merck) and oxalic acid dihydrate (C₂O₄H₂.2H₂O, ≥99 %, Merck) were, consecutively, dissolved in water under reflux conditions (90 °C, 10 min.) in a molar ratio of 3:1 (C₂O₄H₂.2H₂O:NH₄VO₃). The obtained aqueous VO²⁺ solution was then systematically used for the synthesis of both citrato-oxalato-VO²⁺ and citrato-VO²⁺ precursor solutions. For synthesis of an aqueous citrato-oxalato-VO²⁺ precursor solution, citric acid (C₆H₈O₇, 99 %, Sigma-Aldrich) was added to the VO²⁺ solution in a 2:1 molar ratio to VO²⁺. Next, ammonia (NH₃, 32 % aqueous solution, extra pure, Merck) was added, dropwise, to the solution until a pH value of 7 (pH-Electrode, Sentix 60, 3 M KCl) was reached. A nominal vanadium and citrate concentration of 0.1 M and 0.2 M, respectively, was obtained. For synthesis of an aqueous citrato-VO²⁺ precursor solution, a separate solution of ammonium citrate was prepared first by dissolving di-ammonium hydrogen citrate (C₆H₈O₇.2NH₄, ≥99 %, Merck) in water and by adding ammonia to this solution. A nominal citrate concentration of 3 M and a pH value of 7 were experimentally set. Before mixing the VO²⁺ solution with the ammonium citrate solution, the pH of the VO²⁺ solution was increased to a value of 7 by adding ammonia and the volume was adjusted by adding water to achieve a nominal VO²⁺ concentration of 1.5 M. Next, both solutions (1.5 M VO²⁺

solution with a pH value of 7 and 3 M citrate solution with a pH value of 7) were mixed in a volume ratio of 1:1. This mixed solution was aged for 7 days at 4 °C to induce precipitation, which was subsequently removed by filtration (Pall Life Sciences Supor®100 filters with 0.1 μm pore sizes). The precipitate was further washed with water and dried at 60 °C in an air flow furnace. Finally, the pH and volume of the filtrate was adjusted by NH₃ and H₂O to obtain an aqueous citrato-VO²⁺ precursor solution with a pH value of 7. The vanadium and citrate concentration amount 0.1 M and 0.2 M, respectively. Vanadium free solutions of ammonium oxalate and ammonium citrate were prepared as well by the dissolution of ammonium oxalate monohydrate ((COONH₄)₂.H₂O, 99.0-101.0 %, Alfa Aesar) or di-ammonium hydrogen citrate in water, respectively. For both solution solutions, ammonia and water were added to obtain a solution with a pH value of 7 and a nominal oxalate or citrate concentration of 0.3 M.

Solution characterization

All vanadium concentrations were experimentally confirmed by Inductively Coupled Plasma-Atomic Emission Spectrometry (ICP-AES, Perkin Elmer, Optima 3300 DV). The solutions were characterized by liquid state ⁵¹V-NMR (⁵¹Vanadium-Nuclear Magnetic Resonance) and EPR (Electron Paramagnetic Resonance) spectroscopy. All ⁵¹V-NMR spectra were acquired at 78.9 MHz on a Varian Inova 300 spectrometer at room temperature in a 5 mm four-nucleus PFG probe. The chemical shift scale was calibrated at -559.0 ppm with a 0.1 M sodium orthovanadate (Na₃VO₄, 99.9%, Alfa Aesar) solution at pH 12.²⁴ Free induction decays were collected with a 90° pulse of 5.0 μs, a spectral width of 292 kHz, an acquisition time of 0.1 s, a preparation delay of 1 s and 300 accumulations. A line-broadening factor of 5 Hz was applied before Fourier transformation to the frequency domain. X-band continuous-wave (CW) EPR spectra were recorded on a Bruker ESP300E spectrometer (microwave frequency of 9.43 GHz) equipped with a liquid helium cryostat (Oxford Inc.), allowing operation from room temperature down to 2.5 K. The presented CW-EPR spectrum was measured at 100 K using a modulation amplitude of 0.5 mT, a microwave power of 1 mW and a modulation frequency of 100 kHz. The HYSCORE (hyperfine sublevel correlation) spectra²⁵ were recorded on a Bruker Elexsys E500 spectrometer (microwave frequency of 9.76 GHz) equipped with a liquid-helium cryostat (Oxford Inc.). The HYSCORE spectra were measured using the pulse sequence: π/2-τ-π/2-t₁-π-t₂-π/2-τ-echo, with t_{π/2} = 16 ns and t_π = 32 ns; t₁ and t₂ were varied in steps of 16 ns (matrix dimension [350x350]). Spectra were recorded for τ=96 and 172 ns. A four-step phase cycle was performed in all cases to remove unwanted echoes. The HYSCORE traces were baseline corrected using a third-order polynomial, apodized with a Hamming window and zero-filled. After Fourier transformation, the absolute-value spectra were computed and the spectra recorded at different τ values were added together to reduce the blind-spot effect. Simulations of the CW-EPR spectrum were performed with the EasySpin program, a MATLAB toolbox developed for EPR simulations.²⁶

Gel preparation and analysis

The solutions were dried in a Petri dish (air flow furnace, 60 °C).

The obtained powders were analysed by X-Ray Diffraction (XRD) on a Siemens D5000 Diffractometer and by Fourier Transform Infra-Red (FTIR) Spectroscopy on a Bruker, Vertex 70 (128 scans, 4 cm⁻¹ resolution) dispersed in KBr pellets (1 wt. %). The thermal decomposition pathway of the powders was examined by means of Thermo-Gravimetric (TG) analysis. All TG analyses were carried out on the dried powder, heated from room temperature to 625 °C at a heating rate of 10 °C min⁻¹. After sufficient flushing with the analysis gas, the decomposition was studied in dry air or in nitrogen (100 mL min⁻¹). TG analyses were performed on a TA Instruments SDT Q600 (±3 mg of sample).

Phase formation

Both VO²⁺ solutions were spin coated (3000 rpm, 30 s, 1000 rpm/s) onto small pieces (±6 cm²) of p-type Si with 200 nm SiO₂, cleaned in a sulphuric acid peroxide mixture and an ammonia peroxide mixture.²⁷ A hot plate treatment was carried out on each deposited layer at 90 °C and 190 °C (2 minutes). An intermediate anneal was carried out in a rapid thermal anneal system (AccuTherm AW-610), with a chamber flush of 2 minutes, a heating rate of 10 °C s⁻¹, an isothermal period and a slow cooling (> 5 min) in a N₂ environment (10 SLPM). During the isothermal period of 10 minutes, a 0.1 % O₂ ambient condition is obtained by a controlled co-flow (5 SLPM) of high purity N₂ and 1% O₂ (in Ar) and the temperature was set at 400 °C. The deposition cycle (spin coating – hot plate – intermediate anneal) was repeated 4 times. A post deposition anneal was performed in the same rapid thermal anneal system under identical conditions. The temperature and time during the isothermal period of this final anneal were set between 400 °C and 500 °C and at 10 minutes, respectively. The vanadium oxide phase formation was determined by means of XRD on a PANalytical X'pert Pro tool in a Bragg-Brentano configuration with a PIXcel detector in scanning mode (step size 0.0098°). The film morphology was visualized with Scanning Electron Microscopy (SEM, FEI, NOVA 200) in secondary electron imaging mode and a top-down view.

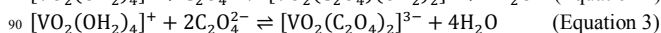
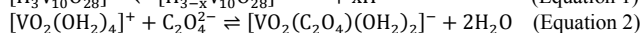
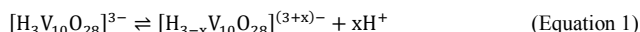
Results and discussion

Synthesis of the citrato(-oxalato)-VO²⁺ precursor solution

The first steps in the synthesis of the aqueous citrato-oxalato-VO²⁺ and citrato-VO²⁺ solution are identical and intend to form VO²⁺ species by a V(V)/V(IV) reduction with oxalic acid as a reducing agent. The dissolution of ammonium metavanadate in water results in a solution with a pH value of 7. According to the ⁵¹V-NMR spectrum, given in Figure 2, the solution is dominated by the presence of tetravanadate species. In addition, penta- and divanadate species are observed in the ⁵¹V-NMR analysis.^{21,28} The relative abundance of each species is determined via peak integration: [V₄O₁₂]⁴⁻ (~67 %), [V₅O₁₅]⁵⁻ (~9 %), [H₂V₂O₇]²⁻ (~13 %) and H₂VO₄⁻ (~11 %). A similar speciation, at pH 7, is reported by McCann et al. for a vanadium concentration of 50 mM.²⁸

Aforementioned vanadate species have a +V oxidation state. However, VO₂ requires a vanadium +IV oxidation state. Hence the vanadium(V) species must be reduced to vanadium(IV) species first. For this reason, oxalic acid is added as a reducing agent.²³ ⁵¹V-NMR is employed to study the V(V)/V(IV)

reduction and to identify the intermediate vanadium species (Figure 3). Firstly, a systematic decrease in the total peak area is observed as function of the oxalic acid molar ratio to vanadium(V), ranging from 0 to 3 (i.e. 0.1 M vanadium (V) and 0 to 0.3 M oxalic acid). This decrease indicates the disappearance of vanadium(V) species in favour of the, paramagnetic and NMR-silent²⁴, vanadium(IV) species and demonstrates the reductive nature of oxalic acid. Simultaneously, the pH drops from 7 to 0.3. Secondly, the chemical shifts in the ⁵¹V-NMR change during the addition of oxalic acid, as observed in Figure 3. Already at an oxalic acid to vanadium molar ratio of 0.25, signals of the tetravanadate species start to diminish and those of the penta-, di- and monovanadate species completely disappear. New peaks in the ⁵¹V-NMR spectra appear at chemical shift values of -422.9, -499.8 and -514.9 ppm, corresponding to the appearance of decavanadate species.²⁸ In such a decavanadate entity, vanadium occupies three different sites, as represented by three different ⁵¹V-NMR signals. The first vanadium site consists of a central and regular VO₆ octahedron, corresponding to a chemical shift at -422.9 ppm. The two other vanadium sites correspond to peripheral tetragonal-pyramidal O=VO₄ units.²⁹ Note that the decavanadate is subjected to acid-base equilibria (Equation 1) with pK_{a1}, pK_{a2} and pK_{a3} equal to 1.9, 4.2 and 6.6, respectively.²⁹ The decavanadate species, present in the solution with a pH value of 6, are dominated by the presence of HV₁₀O₂₈⁵⁻ (with a ratio of 4.2:1 w.r.t. V₁₀O₂₈⁶⁻). Additionally, a signal at -535.7 ppm is observed in the ⁵¹V-NMR spectrum. This one originates from a first oxalate complex, [VO₂(C₂O₄)(OH₂)₂]⁻, formed by oxalate complexation of the VO₂⁺ hydrate in an acidic media (Equation 2).³⁰



As the oxalic acid to vanadium molar ratio increases to 0.75, the peaks corresponding to the peripheral vanadium sites in a decavanadate species shift towards higher field, suggesting their protonation.³¹ At a pH of 2.5, the H₃V₁₀O₂₈³⁻ is the dominating decavanadate species (with a ratio of 4.0:1 w.r.t. H₂V₁₀O₂₈⁴⁻). Simultaneously, the peak height of the signal originating from the [VO₂(C₂O₄)(OH₂)₂]⁻ complex slightly increases. An additional peak is observed at -530.8 ppm, corresponding to a second oxalate complex, [VO₂(C₂O₄)₂]³⁻ (Equation 3).³⁰ Next, at a molar ratio of 1 and 1.5, the decavanadate peaks disappear and only the peak of the [VO₂(C₂O₄)₂]³⁻ complex remains (-530.8 ppm). This last signal diminishes as well when further increasing the oxalic acid to vanadium molar ratio. Finally, at a ratio of 3, no ⁵¹V-NMR signals remain and all vanadium(V) species are reduced.

Since the solution's pH decreases from 7 to 0.3 during the addition of oxalic acid, all the vanadate transformations are associated with the acidification of the aqueous solution and the concurrent oxalate complexation.^{21,31} Both oxalate complexes precede the disappearance of the ⁵¹V-NMR signals and are, hence, considered as the oxidative agents. Their electrochemical potential and the one of the oxalate-free VO₂⁺ are determined by Bruyere et al. (Equations 4 and 5) or estimated using the equilibria listed by Pourbaix et al. (Equation 6)^{32,33}.

$$E_{[\text{VO}_2(\text{C}_2\text{O}_4)]^-/[\text{VO}(\text{C}_2\text{O}_4)]}^0 = 1.13 \text{ V} \quad (\text{Equation 4})$$

$$E_{[\text{VO}_2(\text{C}_2\text{O}_4)_2]^{3-}/[\text{VO}(\text{C}_2\text{O}_4)_2]^{2-}}^0 = 1.22 \text{ V} \quad (\text{Equation 5})$$

$$E_{\text{VO}_2^+/ \text{VO}^{2+}}^0 = 0.77 \text{ V} \quad (\text{Equation 6})$$

The electrochemical potentials associated with the oxalate complexes are higher than the one of the oxalate-free VO_2^+ . Thus, the $\text{VO}_2^+/\text{VO}^{2+}$ reduction is thermodynamically favoured if the VO_2^+ cation is surrounded by one or two bidentate oxalate ligands, and preferably by two. This explains the necessity of an oxalic acid to vanadium molar ratio of 3:1 to ensure a complete reduction of all vanadium(V) species in the aqueous solution.

In conclusion, the addition of oxalic acid results in (i) an acidification of the aqueous solution in which the tetravanadate is converted, via decavanadate, into dioxovanadate and (ii) the formation of oxalato- VO_2^+ complexes. These oxalato- VO_2^+ complexes are considered as the oxidative agents. After the complete reduction process, with an oxalic acid to vanadium ratio of 3, no vanadium(V) species remain.

At this stage, all aqueous vanadium species are successfully converted into VO^{2+} species in which the oxidation state of vanadium equals +IV, as aimed for. To allow chemical solution deposition^{18,27} and to prevent the undesired formation of an insoluble hydroxide, i.e. $\text{VO}(\text{OH})_2$ ²⁹, the VO^{2+} ion must be stabilized in an α -hydroxy-carboxylato- VO^{2+} complex. Such complexes form an amorphous gel by their cross-linking nature (by means of the carboxylate and α -hydroxy functionalities) upon the evaporation of water during the chemical solution deposition process.^{18,27} Therefore citrate is added to the solution as an α -hydroxy-carboxylato, cross-linking complexing agent.^{36–38} Two different solutions are studied: (i) an aqueous citrato-oxalato- VO^{2+} precursor, in which the oxalate groups remain in the solution and (ii) a citrato- VO^{2+} solution whereby the oxalate groups are removed from the solution. In both solutions, the VO^{2+} and citrate concentration equals 0.1 M and 0.2 M, respectively. The citrato- VO^{2+} solution is expected to have an advantage over the citrato-oxalato- VO^{2+} solution since fewer carbon atoms must be, thermally, removed during vanadium oxide phase formation.

In the synthesis of the aqueous citrato-oxalato- VO^{2+} solution, citric acid and NH_3 are directly added to the aqueous oxalato- VO^{2+} solution (Figure 1). The obtained pH value of 7 guarantees the deprotonation of citric acid's carboxylic acid groups (pK_a : 6.4)³⁷, ensuring the formation of citrato-oxovanadate(IV) complexes. In the synthesis of the aqueous, oxalate-free citrato- VO^{2+} solution, the removal of oxalate ions is aimed for. Here, the pH and the VO^{2+} concentration of the oxalato- VO^{2+} solution is adjusted to 7 and 1.5 M, respectively, by the addition of NH_3 and water (Figure 1). This solution is then mixed with a 3 M citrate solution, having a pH of 7, in a 1:1 volume ratio to maintain the 2:1 molar ratio of citrate ions to the VO^{2+} species (Figure 1). From this mixed solution, ammonium oxalate precipitates, as proven by its XRD analysis in Figure 4 and its FTIR spectrum in Figure S1[†]. No vanadyl stretching vibrations, i.e. $\nu(\text{V}^{4+}=\text{O})$ or $\nu(\text{V}^{5+}=\text{O})$, are observed around 960 or 1020 cm^{-1} , suggesting that the precipitate is vanadium free.^{23,38} The ammonium oxalate precipitate is filtrated from the solution and the synthesis of the citrato- VO^{2+} solution is finalised by adding NH_3 to re-adjust the pH to a value of 7.

Structural investigation of the VO^{2+} complexation by citrate

At this point a procedure for the synthesis of an aqueous citrato-oxalato- VO^{2+} and an aqueous oxalato-poor citrato- VO^{2+} solution is presented. Before discussing the difference in their thermal decomposition pathway and its consequence on the vanadium oxide phase formation; the direct environment of the VO^{2+} ion in the citrato- VO^{2+} complex will be elucidated. Firstly, the current knowledge on the complexation of citric acid and its pH-dependent derivatives with the VO^{2+} ion, in the solid state^{39–42} and in the solution^{40,43,44}, is briefly highlighted. The formation of dimeric structures with composition $[(\text{VO})_2(\text{C}_6\text{H}_4\text{O}_7)_2]^{4-}$ is generally accepted in or from solutions with, approximately, an equimolar ligand: VO^{2+} ratio and a neutral pH value.^{39–44} Note that (i) the VO^{2+} coupling into a dimeric structure is realised by two deprotonated α -hydroxyl groups each originating from one citrate ligand in the dimeric composition and (ii) each citrate ligand chelates a first VO^{2+} ion by two carboxylate groups and a second VO^{2+} ion with one carboxylate group which leads to a sixfold chelating of each V centre without free available carboxylate groups. In these solution studies, the vanadium concentration is limited ($\sim 10^{-3}$ M)^{43,44} and ammonium is not present or actively removed^{40,43,44}. In this work, the formation of ammonium carboxylate interactions, bridging two or more citrato- VO^{2+} complexes into a network is aimed for. This cross-linked network of citrato- VO^{2+} complexes will allow the formation of an amorphous gel upon the evaporation of water during the chemical solution deposition process.^{18,27} For this purpose, a higher vanadium concentration (two orders in magnitude) is set and ammonium is, deliberately, added to the solution.

Figure 5 shows the experimental and simulated X-band CW-EPR spectra recorded at 100 K for the oxalate-free citrato- VO^{2+} precursor solution. Firstly, the anisotropic spectrum exhibits a multiline pattern, corresponding to a chelated VO^{2+} system with an axial symmetry⁴⁵, with a well resolved hyperfine structure and without a superimposed broad feature. However, Kiss et al. report X-band EPR spectra recorded on frozen solutions with such a broad feature and ascribe this broad feature to the presence of paramagnetic dimeric structures.⁴³ According to Chasteen et al. and Smith et al., a broad feature, superimposed on a multiline spectrum, is characteristic for VO^{2+} clusters or dipolarly interacting VO^{2+} centres.^{45,46} The absence of this broad feature in the X-band EPR spectrum, shown in Figure 5, indicates the presence of mononuclear VO^{2+} entities in the frozen citrato- VO^{2+} solution similar to the observations of Garriba et al. and Buglyo et al. in the case of mononuclear VO^{2+} complexes with alternative carboxylate based ligands^{47,48}. Note that dimeric citrato- VO^{2+} complexes could be present without exhibiting a feature in the EPR spectrum if they would be antiferromagnetically coupled. This contradicts the observations of Kiss et al.⁴³ and is considered unlikely. Thus, the X-band spectrum, shown in Figure 5, stems from mononuclear VO^{2+} complexes present in the citrato- VO^{2+} solution. Secondly, the principal g and ^{51}V hyperfine values are determined for this mononuclear VO^{2+} complex by simulation of the experimental CW-EPR spectrum: $g_{x,y} = 1.976$, $g_z = 1.944$ and $A_{x,y} = 179 \pm 5$ MHz and $A_z = 500 \pm 5$ MHz. The g_z and A_z values are sensitive to the direct environment of the oxovanadate(IV) ion and allow, in combination with the additivity relationship, a prediction of the equatorial ligation types to the oxovanadate(IV) ion.^{45,46} The principal g and ^{51}V hyperfine values of

[VO(H₂O)₅]²⁺, 1.933 (g_z) and 547 MHz (A_z)⁴⁵, differ from those observed for the citrato-VO²⁺ solution. The consecutive replacement of H₂O molecules by R-CO₂⁻ ligands decreases the A_z value^{45,46}. The theoretical value for an all (i.e. fourfold) R-CO₂⁻ ligation (i.e. 512 MHz) best fits the simulated ⁵¹V hyperfine value. Additionally, the simulated principal g and ⁵¹V hyperfine values differ significantly from those obtained by Kiss et al. in the case of dimeric citrato-VO²⁺ complexes (i.e. g_z = 1.953 and A_z = 231 MHz)⁴³ which stresses the different structure of the citrato-VO²⁺ complexes in this work. Contrarily, the simulated values correspond well to those of mononuclear carboxylato-VO²⁺ complexes with an axial symmetry such as the glycolato-VO²⁺ reported by Garribba et al. (g_{x,y} = 1.980, g_z = 1.941, A_{x,y} = 180 MHz and A_z = 505 MHz)⁴⁷. Summarizing, the observed X-band EPR spectrum and its simulated principal g and ⁵¹V hyperfine values are ascribed to the presence of mononuclear VO²⁺ complexes, with an axial symmetry and a four R-CO₂⁻ ligation at the equatorial positions, present in the citrato-VO²⁺ solution. Note that the presence of oxalato-VO²⁺ complexes would result in g_{x,y} = 1.966, g_z = 1.939, A_{x,y} = 295 MHz and A_z = 515 MHz⁴⁸, and is therefore excluded.

To elucidate the structure of these mononuclear VO²⁺ complexes in more detail, pulsed EPR experiments are performed on the citrato-VO²⁺ solution. HYSORE experiments are performed at a magnetic-field setting known to excite all molecular orientations. The HYSORE spectrum, depicted in Figure 6, reveals only a weak hyperfine coupling with protons (maximum coupling 2.5 MHz in magnitude). The hyperfine coupling of protons present in equatorially or axially ligated water or hydroxyl groups is expected to be much larger.⁴⁹ The small proton hyperfine value is consistent with proton nuclei further away from the oxovanadate(IV) centre, as is expected in the case of R-CO₂⁻ ligation. In addition, the lack of clear cross peaks due to interactions with ¹⁴N nuclei excludes ammonia ligation. Thus, the HYSORE data indicates that neither water, nor hydroxyl groups or ammonia are involved in the ligation of the oxovanadate(IV) ion and thus this data supports the all equatorial, R-CO₂⁻ ligation.

In conclusion, the EPR and HYSORE characteristics demonstrate the mononuclear structure of present citrato-VO²⁺ complexes and, hence, the successful annihilation of the, frequently reported, dimeric structure. In such a mononuclear citrato-VO²⁺ complex, the VO²⁺ ions is ligated by four R-CO₂⁻ groups at the equatorial positions and likely a fifth R-CO₂⁻ group at the axial position. Additional information on the structure of the citrato-VO²⁺ complexes and its interaction with ammonium groups linking the excess citrate, is given by FTIR spectroscopy (Figure S3[†] and Table S4[†]).

Thermal decomposition

With the identification of the mononuclear citrato-VO²⁺ complexes, ligated by four or five R-CO₂⁻ groups, all is set to discuss the thermal decomposition pathway of the citrato-VO²⁺ and the citrato-oxalato-VO²⁺ gel. Because, the actual vanadium oxide phase formation will occur in a low pO₂ ambient²³, the thermal decomposition pathway of both precursor gels is studied in N₂. Figure 7 shows the mass profile (TGA), its derivative (DTG) and the associated heat flow of both precursor gels up to 625 °C. For both gels, the largest, endothermic and non-oxidative

decomposition step is observed between 125 °C and 200 °C with its decomposition rate maximum at 151 °C. According to Van Werde et al., this results from the decomposition of the excess of ammonium citrate by a series of reactions in which (i) citrate's α-hydroxyl functionality is dehydroxylated, (ii) NH₃ is released by the decomposition of ammonium carboxylate groups into carboxylic acid groups and (iii) the formed carboxylic acid groups either decarboxylate or react with the gaseous NH₃ in the formation of amide groups.³⁴ As the temperature exceeds 200 °C, the thermal decomposition profile of both precursor gels diverges. Between 200 and 300 °C, the citrato-oxalato-VO²⁺ gel exhibits a larger weight loss with two additional, local decomposition rate maximum (i.e. at 210 °C and 265 °C). This additional weight loss is assigned to the decomposition of oxalate residues, present in the citrato-oxalato-VO²⁺ gel, with the release of CO₂ and H₂O. In case of the citrato-oxalato-VO²⁺ gel, the final decomposition step is already between 300 and 400 °C with its local decomposition rate maximum at 345 °C. For the citrato-VO²⁺ gel, this final decomposition step is shifted to 500 °C, with its local decomposition rate maximum at 445 °C.

The expected difference in the thermal decomposition pathway between the citrato-VO²⁺ and the citrato-oxalato-VO²⁺ gel is indeed observed. (i) The reduced amount of carbon atoms in the citrato-VO²⁺ gel, leads to smaller total weight loss (i.e. 72 %) in comparison to the one of the citrato-oxalato-VO²⁺ gel (i.e. 78 %). (ii) The temperature of the final decomposition step of the citrato-VO²⁺ gel is clearly extended with about 100 °C in comparison to the one of the citrato-oxalato-VO²⁺ gel.

Phase formation

The synthesized aqueous citrato-oxalato-VO²⁺ and citrato-VO²⁺ solutions are spin coated on SiO₂ for the formation of four layered vanadium oxide films. Multiple thermal treatments are applied to convert the spin coated precursor solution into an oxide film. (i) A hot plate treatment is performed at 90 °C and at 190 °C in ambient conditions. As discussed during the thermal decomposition study, the ammonium citrate excess is decomposed during this treatment. (ii) Secondly, an intermediate anneal is applied at 400 °C for 10 minutes in a 0.1 % O₂ ambient. This intermediate anneal enables the subsequent deposition of layers without affecting the previously deposited layer and the V(IV) oxidation state.²³

Figure 8 shows the XRD patterns of the vanadium oxide films from the aqueous citrato-oxalato-VO²⁺ and citrato-VO²⁺ solution. For the citrato-oxalato-VO²⁺ precursor solution, the initial four layered film (labelled 'As deposited' in Figure 8) already shows an onset for monoclinic VO₂ B phase formation, indicated by the presence of the (001) and (002) diffraction peaks at 14.4 °2θ and 29.0 °2θ, respectively (JCPDS 81-2392)⁵⁰. After applying a post deposition anneal at 400 °C in a 0.1 % O₂ ambient, the integrated area of the diffraction peaks at 14.4 °2θ and 29.0 °2θ slightly increases, suggesting growth of the amount of crystalline material. After an anneal at 450 °C in a 0.1 % O₂ ambient, the diffraction peaks associated with monoclinic VO₂ disappear and diffraction peaks corresponding to monoclinic V₆O₁₃ arise at 26.8 °2θ (003) and 45.9 °2θ (005) (JCPDS 78-0983)⁵⁰. As the temperature further increases to 500 °C, the integrated area of the diffraction peak at 26.8 °2θ increases and additional diffraction peaks for monoclinic V₆O₁₃ are being observed at 17.8 °2θ (002)

and $36.0^\circ 2\theta$ (004), suggesting an increased amount of crystalline material and a strongly textured film. Besides the diffraction peaks associated with crystalline, monoclinic V_6O_{13} , also a peak at $27.9^\circ 2\theta$ is observed. This peak can be assigned to the (220) diffraction peak of monoclinic VO_2 M1 (JCPDS 71-4821)⁵⁰. Thus, the aqueous citrato-oxalato- VO_2^{2+} solution, containing ammonium oxalate residues, results in a crystalline VO_2 B film after an intermediate anneal at $400^\circ C$, which further evolves to V_6O_{13} after an additional post deposition anneal at 450 or $500^\circ C$. Studies of Murphy et al.¹¹ and Premkumar et al.¹⁴ support our observed transformation of crystalline VO_2 B to crystalline V_6O_{13} as function of temperature.

The crystallisation behaviour of the citrato- VO_2^{2+} variant clearly differs from those of the citrato-oxalato- VO_2^{2+} precursor solution (Figure 8). Since the XRD pattern of the initial four layered film does not show any diffraction, this film is considered amorphous. After a post deposition anneal at $400^\circ C$ or $450^\circ C$, for 10 minutes in a 0.1% O_2 ambient, the film stays amorphous. As the temperature increases to $500^\circ C$, crystallisation into the VO_2 monoclinic (M1) phase is observed, as evidenced by the diffraction peaks at $27.9^\circ 2\theta$ (110) and $57.6^\circ 2\theta$ (220). No additional peaks are observed in the XRD pattern, suggesting that the film consists of phase pure, monoclinic VO_2 M1. The crystallisation of an amorphous vanadium oxide layer into monoclinic VO_2 M1 on SiO_2 in a low pO_2 ambient at temperatures around $500^\circ C$ is in agreement with previous reports.^{7,14}

In conclusion, the difference in the chemistry and composition of the aqueous VO_2^{2+} solution (i.e. the presence or absence of oxalate residues), drastically alters the vanadium oxide phase formation. (i) The aqueous citrato-oxalato- VO_2^{2+} precursor solution results in crystalline VO_2 B at $400^\circ C$ and mainly V_6O_{13} at 450 and $500^\circ C$. (ii) The aqueous oxalate-free citrato- VO_2^{2+} precursor solution leads to an amorphous film below $500^\circ C$ and to crystalline, phase pure VO_2 M1 at $500^\circ C$. According to Schwartz et al., the formation of crystallites preferentially occurs if the majority of the organic matrix is removed.⁵¹ This requirement is fulfilled at $400^\circ C$ for the citrato-oxalato- VO_2^{2+} precursor solution and at $500^\circ C$ for the citrato- VO_2^{2+} solution (Figure 7). Thus, in case of the citrato-oxalato- VO_2^{2+} precursor solution, the oxalate residues induce a lower final decomposition temperature which results in an earlier crystallization. At these specific conditions (i.e. $400^\circ C$, 0.1% O_2 and a SiO_2 surface) VO_2 B crystallizes. This VO_2 B is subjected to further oxidation as the temperature increases. In case of the citrato- VO_2^{2+} , no crystallization occurs below $500^\circ C$ and the VO_2 B crystallization window is overpassed. These new conditions (i.e. $500^\circ C$, 0.1% O_2 and a SiO_2 surface) lead to the direct transformation of an amorphous vanadium oxide layer into crystalline VO_2 M1.

Morphology of the VO_2 M1

Besides the crystallinity, the morphology of the obtained VO_2 M1 is of interest. The temperature dependant morphology is studied by SEM in Figure 9. The as deposited film obtained after an intermediate anneal at $400^\circ C$, shows a continuous and featureless morphology. The films annealed at $400^\circ C$ and $450^\circ C$ become discontinuous and the VO_2 transforms into islands. As the temperature increases to $500^\circ C$ and crystallisation into the monoclinic VO_2 M1 phase occurs (Figure 8), the films'

morphology changes into randomly distributed particles. The total substrate coverage amounts to 48% . The formation of VO_2 particles from a thin (< 20 nm), amorphous and continuous film deposited on SiO_2 , is consistent with previous observations reported by Suh et al. and Nag et al.^{5,6} Solid state de-wetting of the metastable VO_2 film and the subsequent Ostwald ripening into VO_2 particles was the suggested explanation. This process is, thermodynamically, driven by surface energy minimization and can occur via surface diffusion well below the film's melting temperature, especially when the film is very thin.⁵²

Conclusion

An aqueous precursor solution containing citrato- VO_2^{2+} complexes is synthesized for the formation of monoclinic VO_2 M1 particles on SiO_2 . Firstly, the synthesis of the aqueous citrato-oxovanadate(IV) solution is studied by ^{51}V -NMR. During synthesis, cyclic tetravanadate(V) is converted into VO_2^{2+} using oxalic acid as an acidifier and reducing agent. The subsequent complexation of the VO_2^{2+} ion with citrato complexing agents and the differentiation between a citrato-oxalato- VO_2^{2+} and an oxalate-free citrato- VO_2^{2+} solution is studied by EPR and FTIR spectroscopy: (i) A successful procedure based on the limited solubility of $(NH_4)_2C_2O_4$ in water, is developed for the removal of the oxalate excess (which was necessary for a complete VO_2^+/VO_2^{2+} reduction). (ii) In both solutions, the VO_2^{2+} ion is anchored in a mononuclear and distorted octahedral complex with a four $R-CO_2^-$ ligation at the equatorial positions and likely a fifth $R-CO_2^-$ ligation at the axial position. Secondly, both precursor solutions are successfully used for the preparation of crystalline vanadium oxide nanostructures on SiO_2 , after a thermal anneal in a 0.1% O_2 ambient. The aqueous citrato-oxalato- VO_2^{2+} precursor solution results in crystalline VO_2 B at $400^\circ C$ and mainly V_6O_{13} at 450 and $500^\circ C$. The aqueous, oxalate-free citrato- VO_2^{2+} precursor solution leads to an amorphous film below $500^\circ C$ and to crystalline, phase pure VO_2 M1 at $500^\circ C$. The difference in phase formation is ascribed to the differentiated thermal decomposition pathway, caused by the presence or absence of oxalate residues. Thus, by optimizing the chemical composition in the aqueous precursor solution, the final vanadium oxide stoichiometry and phase (obtained after solution deposition and film processing at specific conditions) can be controlled.

Acknowledgements

N. Peys and E. Peeters are doctoral, and C. De Dobbelaere is a postdoctoral research fellow of the Research Foundation Flanders (FWO-Vlaanderen). The Hercules Foundation is acknowledged for the financial support for the Bruker Elexsys E500 EPR spectrometer upgrade. S. Van Doorslaer and P. Adriaensens thank the research community project MULTIMAR (Multidisciplinary Magnetic Resonance) of the Research Foundation Flanders (FWO-Vlaanderen) for their support. The authors are indebted to J. D'Haen, B. Ruttens and K. Schellens for the powder analyses.

Notes and references

^a Hasselt University, Institute for Materials Research, Inorganic and Physical Chemistry, Diepenbeek, Belgium;

- ^b IMEC vzw, Heverlee, Belgium;
- ^c Hasselt University, Institute for Materials Research, Applied and Analytical Chemistry, Diepenbeek, Belgium;
- ^d University of Antwerp, Department of Physics, BIMEF Laboratory, Antwerp, Belgium;
- ^e IMEC vzw, Division IMOMECE, Diepenbeek, Belgium;
- ^f KULeuven, Lab for Physical and Analytical Chemistry, Heverlee, Belgium;
- * Author information: Hasselt University, Institute for Materials Research, Inorganic and Physical Chemistry, Diepenbeek, Belgium, Tel: +31 11268307, E-mail: marlies.vanbael@uhasselt.be;
- † Electronic Supplementary Information (ESI) available: [Figure S1 and S3: Fourier Transform Infra-Red spectra; Table S2 and S4: Band assignments of the main vibrations of the Fourier Transform Infra-Red spectra]
- H. A. Wriedt, *Bull. Alloy Phase Diagrams*, 1989, **10**, 1989.
 - Y. Wang and G. Cao, in *Handbook of Nanoceramics and Their Based Nanodevices: Synthesis and Processing*, eds. T.-Y. Tseng and H. S. Nalwa, American Scientific Publishers, 1st edn., 2009, pp. 97–123.
 - F. J. Morin, *Phys. Rev. Lett.*, 1959, **3**, 34–36.
 - C. G. Granqvist, *Sol. Energy Mater. Sol. Cells*, 2007, **91**, 1529–1598.
 - J. Nag and R. F. Haglund, *J. Phys. Condens. Mater*, 2008, **20**, 264016.
 - J. Y. Suh, R. Lopez, L. C. Feldman, and R. F. Haglund, *J. Appl. Phys.*, 2004, **96**, 1209–1214.
 - S. A. Pauli, R. Herger, P. R. Willmott, E. U. Donev, J. Y. Suh, and R. F. Haglund, *J. Appl. Phys.*, 2007, **102**, 073527.
 - M. S. Whittingham, Y. Song, S. Lutta, P. Y. Zavalij, and N. A. Chernova, *J. Mater. Chem.*, 2005, **15**, 3362–3379.
 - H. Li, P. He, Y. Wang, E. Hosono, and H. Zhou, *J. Mater. Chem.*, 2011, **21**, 10999.
 - J. Höwing, T. Gustafsson, and J. O. Thomas, *Acta Crystallogr. B.*, 2003, **59**, 747–752.
 - D. W. Murphy and P. A. Christian, *Science (80-.)*, 1979, **205**, 651–656.
 - B. C. Piccirillo, R. Binions, and I. P. Parkin, *Chem. Vap. Depos.*, 2007, **13**, 145–151.
 - G. Rampelberg, M. Schaekers, K. Martens, Q. Xie, and D. Deduytsche, *Appl. Phys. Lett.*, 2011, **98**, 162902.
 - P. A. Premkumar, M. Toeller, I. P. Radu, C. Adelman, M. Schaekers, J. Meersschaut, T. Conard, and S. Van Elshocht, *ECS J. Solid State Sci. Technol.*, 2012, **1**, 169–174.
 - R. Lopez, R. F. Haglund, L. C. Feldman, L. A. Boatner, and T. E. Haynes, *Appl. Phys. Lett.*, 2004, **85**, 5191–5194.
 - Z. Luo, Z. Wu, T. Wang, X. Xu, W. Li, W. Li, and Y. Jiang, *J. Phys. Chem. Solids*, 2012, **73**, 1122–1126.
 - Y. Cui and S. Ramanathan, *J. Vac. Sci. Technol. A Vacuum, Surfaces, Film.*, 2011, **29**, 041502.
 - H. Van den Rul, M. K. Van Bael, A. Hardy, K. Van Werde, and J. Mullens, in *Handbook of Nanoceramics and Their Based Nanodevices: Synthesis and Processing*, eds. T.-Y. Tseng and H. S. Nalwa, American Scientific Publishers, 1st edn., 2009, pp. 267–300.
 - D. P. Partlow, S. R. Gurkovich, K. C. Radford, and L. J. Denes, *J. Appl. Phys.*, 1991, **70**, 443–452.
 - B.-G. Chae, H.-T. Kim, S.-J. Yun, B.-J. Kim, Y.-W. Lee, and K.-Y. Kang, *Jpn. J. Appl. Phys.*, 2007, **46**, 738–743.
 - J. Livage, *Chem. Mater.*, 1991, **3**, 578–593.
 - Y. Dachuan, X. Niankan, Z. Jingyu, and Z. Xiulin, *J. Phys. D. Appl. Phys.*, 1996, **29**, 1051–1057.
 - N. Peys, Y. Ling, D. Dewulf, S. Gielis, C. De Dobbelaere, D. Cuyppers, P. Adriaensens, S. Van Doorslaer, S. De Gendt, A. Hardy, and M. K. Van Bael, *Dalt. Trans.*, 2013, **42**, 959–968.
 - D. Rehder, *Coord. Chem. Rev.*, 2008, **252**, 2209–2223.
 - P. Höfer, A. Grupp, H. Nebenführ, and M. Mehring, *Chem. Phys. Lett.*, 1986, **132**, 279–282.
 - S. Stoll and A. Schweiger, *J. Magn. Reson.*, 2006, **178**, 42–55.
 - M. K. Van Bael, D. Nelis, A. Hardy, D. Mondelaers, K. Van Werde, J. D'Haen, G. Vanhoyland, H. Van den Rul, J. Mullens, L. C. Van Poucke, F. Frederix, and D. J. Wouters, *Integr. Ferroelectr.*, 2002, **45**, 113–122.
 - N. Mccann, M. Wagner, and H. Hasse, *Dalt. Trans.*, 2013, **42**, 2622–2628.
 - D. Rehder, *Dalt. Trans.*, 2013, **42**, 11749–11761.
 - P. M. Ehde, I. Andersson, and L. Pettersson, *Acta Chem. Scand.*, 1989, **43**, 136–143.
 - A. Gorzsás, K. Getty, I. Andersson, and L. Pettersson, *Dalton Trans.*, 2004, 2873–82.
 - M. Pourbaix, *Atlas of Electrochemical Equilibria in Aqueous Solutions*, National Association of Corrosion Engineers, Houston, 1974.
 - V. I. E. Bruyère, L. A. García Rodenas, P. J. Morando, and M. A. Blesa, *J. Chem. Soc. Dalt. Trans.*, 2001, 3593–3597.
 - K. Van Werde, D. Mondelaers, G. Vanhoyland, D. Nelis, and M. K. Van Bael, *J. Mater. Sci.*, 2002, **37**, 81–88.
 - A. Hardy, S. Van Elshocht, D. Dewulf, S. Clima, N. Peys, C. Adelman, K. Opsomer, P. Favia, H. Bender, I. Hoflijik, T. Conard, A. Franquet, H. Van den Rul, J. a. Kittl, S. De Gendt, M. K. Van Bael, and J. Mullens, *J. Electrochem. Soc.*, 2010, **157**, G13.
 - D. Dewulf, N. Peys, S. Van Elshocht, G. Rampelberg, C. Detavernier, S. De Gendt, a. Hardy, and M. K. Van Bael, *Microelectron. Eng.*, 2011, **88**, 1338–1341.
 - D. R. Lide, *Handbook of Chemistry and Physics*, 83rd edn., 2002.
 - C. Djordjevic, P. L. Wilkins, E. Sinn, and R. J. Butcher, *Inorg. Chem.*, 1995, **230**, 241–244.
 - M. Velayutham, B. Varghese, and S. Subramanian, *Inorg. Chem.*, 1998, **37**, 1336–1340.
 - S. Burojevic, I. Shweky, A. Bino, D. A. Summers, and R. C. Thompson, *Inorg. Chim. Acta*, 1996, **251**, 75–79.
 - Z. Zhou, H. Wan, S. Hu, and K. Tsai, *Inorg. Chim. Acta*, 1995, **237**, 193–197.
 - M. Tsaramyrsi, M. Kaliva, and A. Salifoglou, *Inorg. Chem.*, 2001, **40**, 5772–5779.
 - T. Kiss, P. Buglyó, D. Sanna, G. Micera, P. Decock, and D. Dewaele, *Inorganica Chim. Acta*, 1995, **239**, 145–153.
 - S. Berto, P. G. Daniele, E. Prentesi, and E. Laurenti, *Inorganica Chim. Acta*, 2010, **363**, 3469–3476.
 - N. D. Chasteen, in *Biological Magnetic Resonance*, 1981, pp. 53–119.
 - T. S. Smith, R. Lobrutto, and V. L. Pecoraro, 2002, **228**, 1–18.
 - E. Garribba, G. Micera, A. Panzaneli, and D. Sanna, *Inorg. Chem.*, 2003, **42**, 3981–7.
 - P. Buglyó, E. Kiss, I. Fábíán, T. Kiss, D. Sanna, E. Garribba, and G. Micera, *Inorganica Chim. Acta*, 2000, **306**, 174–183.
 - S. C. Larsen, *J. Phys. Chem. A*, 2001, 8333–8338.
 - JCPDS, *Powder diffraction file of inorganic phases*, Swarthmore, 1997.
 - R. W. Schwartz, T. Schneller, and R. Waser, *Compte Rendus Chim.*, 2004, **7**, 433–461.
 - C. V Thompson, *Annu. Rev. Mater. Res.*, 2012.

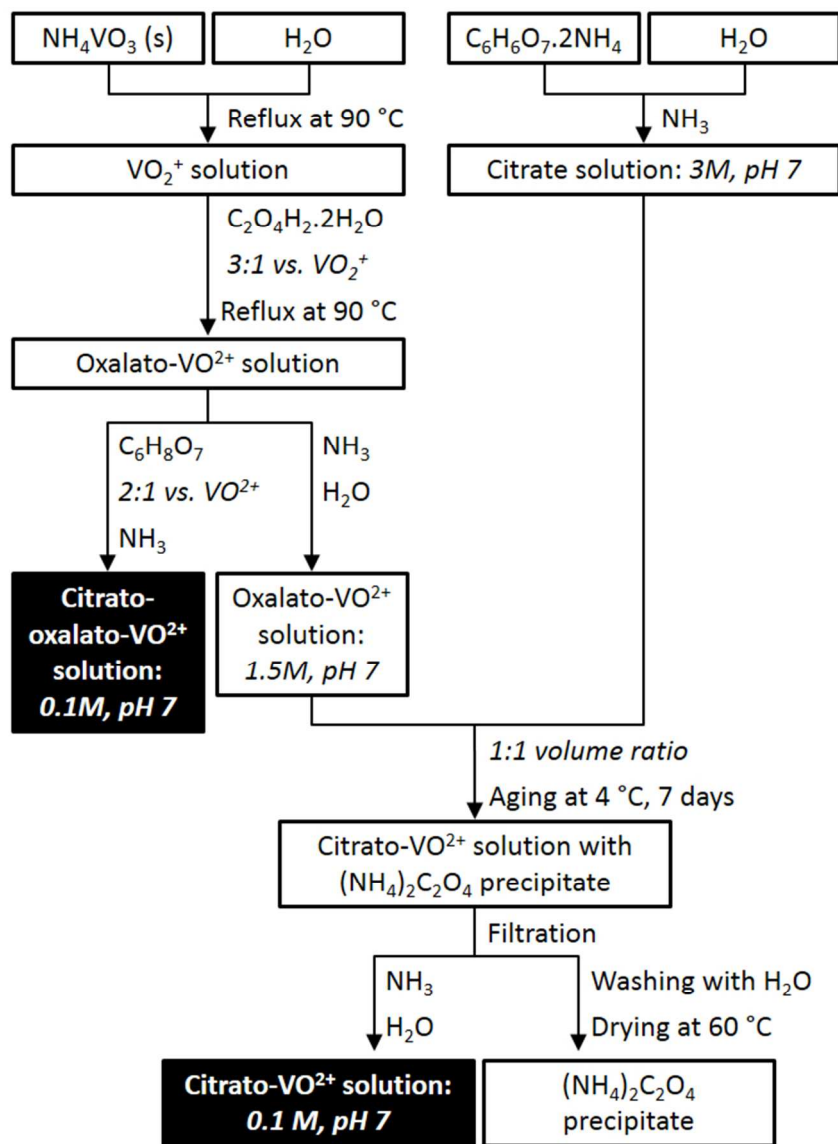


Figure 1: Schematic representation for the synthesis of the aqueous citrato-oxalato-VO₂⁺ and citrato-VO₂⁺ precursor solutions. All ratios are molar ratios, unless specified otherwise. Both solutions have a VO₂⁺ and citrate concentration of 0.1 M and 0.2 M, respectively.
190x254mm (96 x 96 DPI)

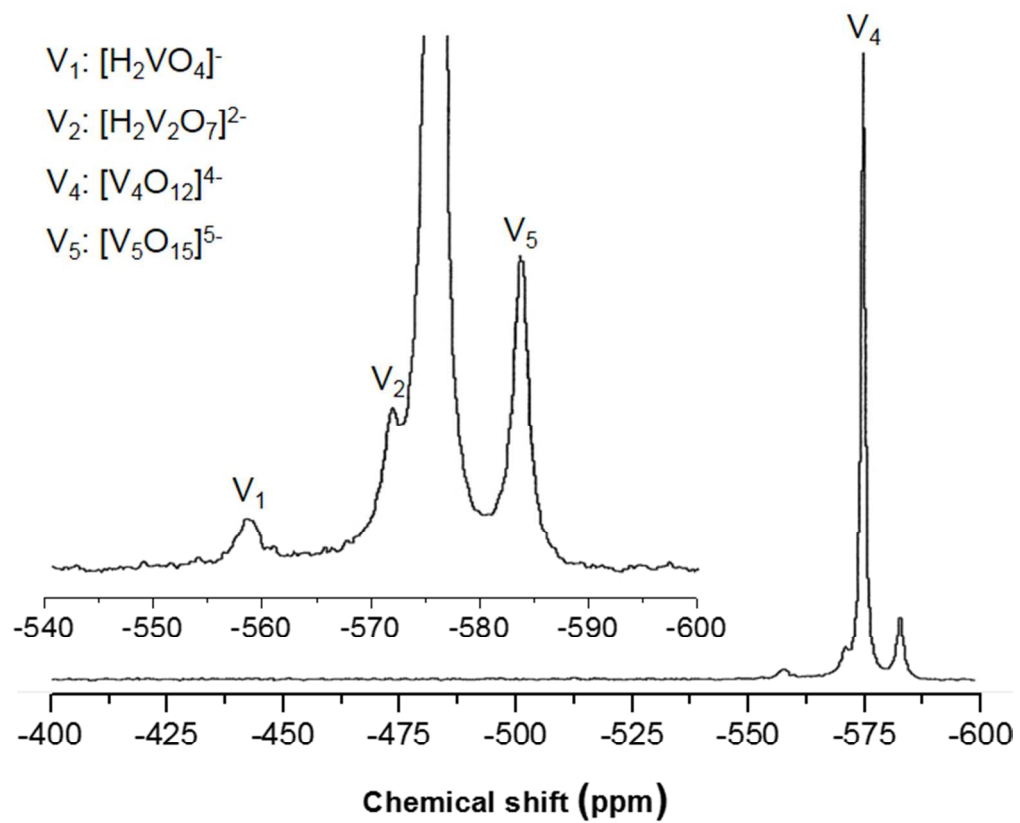


Figure 2: ^{51}V -NMR of the vanadium(V) species present in the aqueous solution immediately after the dissolution of ammonium metavanadate in water. The assignments are based on references [25,29].
190x160mm (96 x 96 DPI)

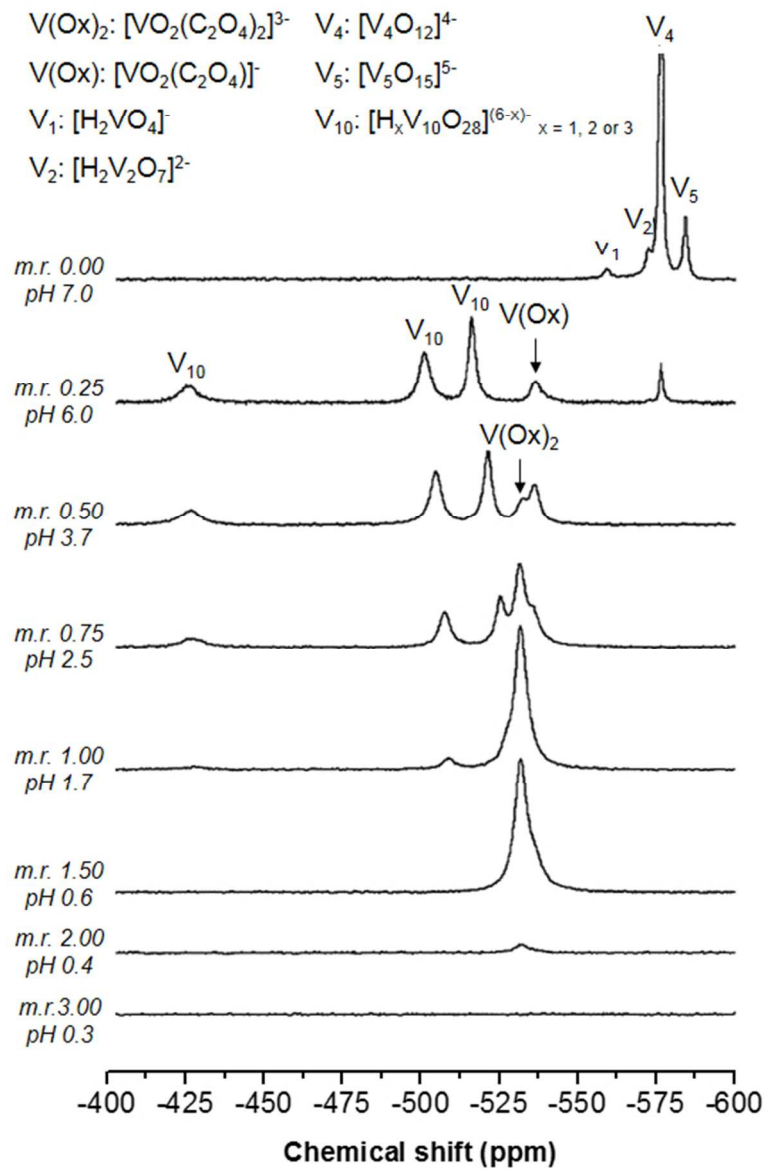


Figure 3: ^{51}V -NMR of the vanadium(V) species present in the aqueous solution after the addition of oxalic acid with an increasing molar ratio (m.r.) to V(V). Besides the NMR spectrum, the pH value of the considered solution is indicated. The peak assignments are based on reference [25,29,31].
142x223mm (96 x 96 DPI)

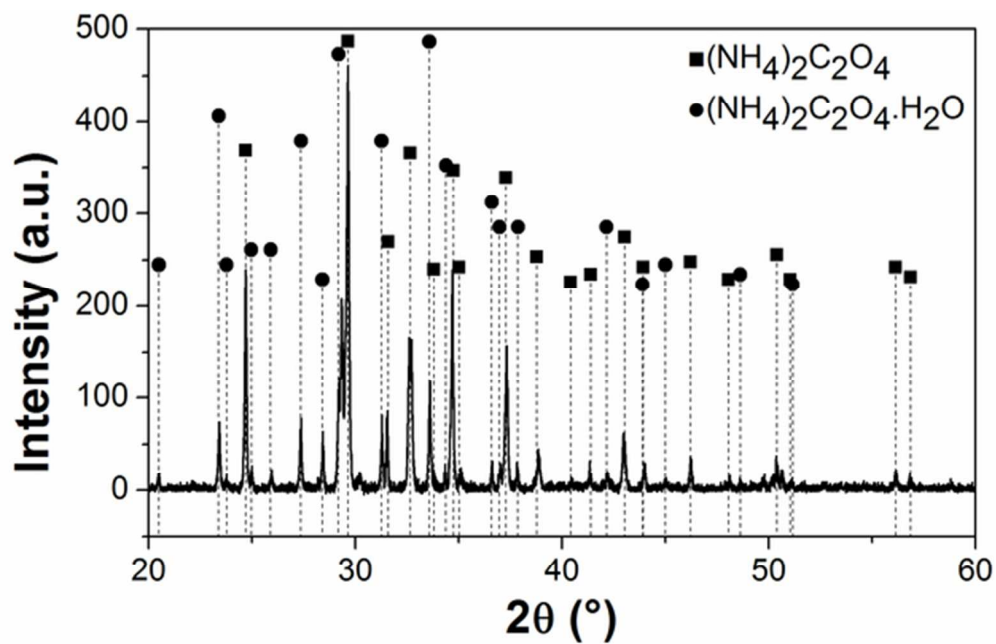


Figure 4: X-Ray Diffraction pattern of the precipitate originating from the synthesis of the aqueous citrato- VO^{2+} precursor solution. The assignments are based on JCPDS 44-0724 for $(\text{NH}_4)_2\text{C}_2\text{O}_4$ and JCPDS 14-0801 for $(\text{NH}_4)_2\text{C}_2\text{O}_4 \cdot \text{H}_2\text{O}$ (reference [50]).
53x34mm (300 x 300 DPI)

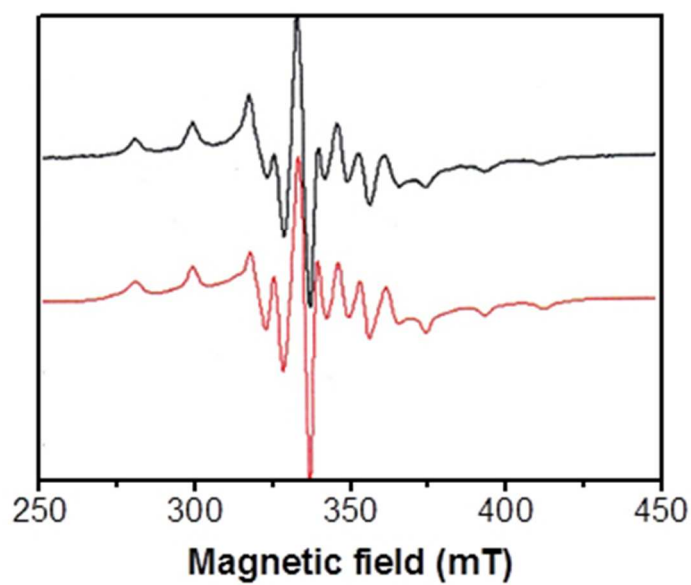


Figure 5: Experimental (black) and simulated (red) X-band CW-EPR spectra of the frozen citrato-VO²⁺ precursor solutions taken at 100 K. The simulated spectrum is obtained using the following principal g and ⁵¹V hyperfine values: 1.976 (g_x), 1.976 (g_y), 1.944 (g_z), 179 ± 5 MHz (A_x), 179 ± 5 MHz (A_y) and 500 ± 5 MHz (A_z).

101x83mm (96 x 96 DPI)

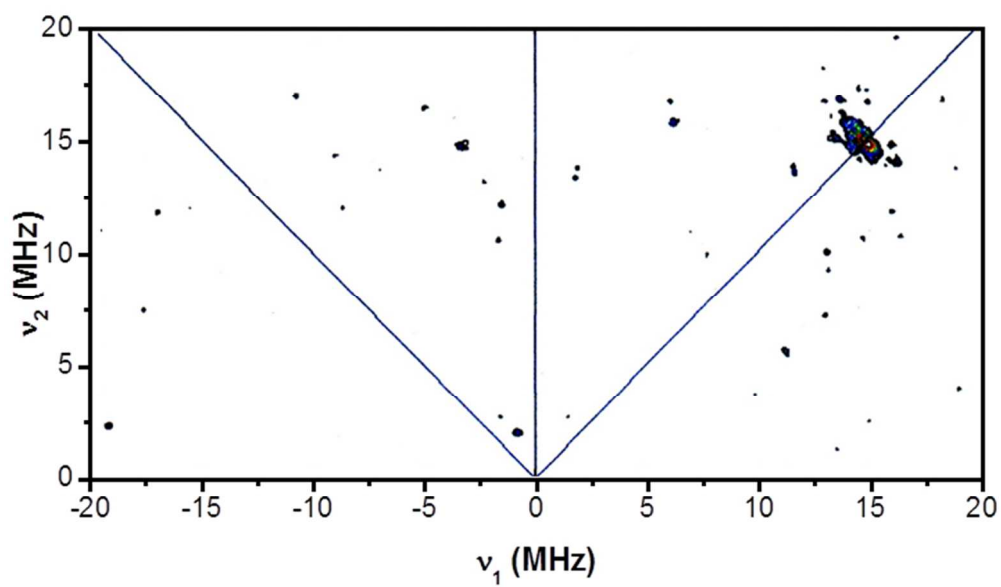


Figure 6: Experimental HSCORE spectrum of the frozen citrato-VO²⁺ precursor solution taken at observer position $B_0 = 347$ mT at which all molecular orientations are excited.
190x114mm (96 x 96 DPI)

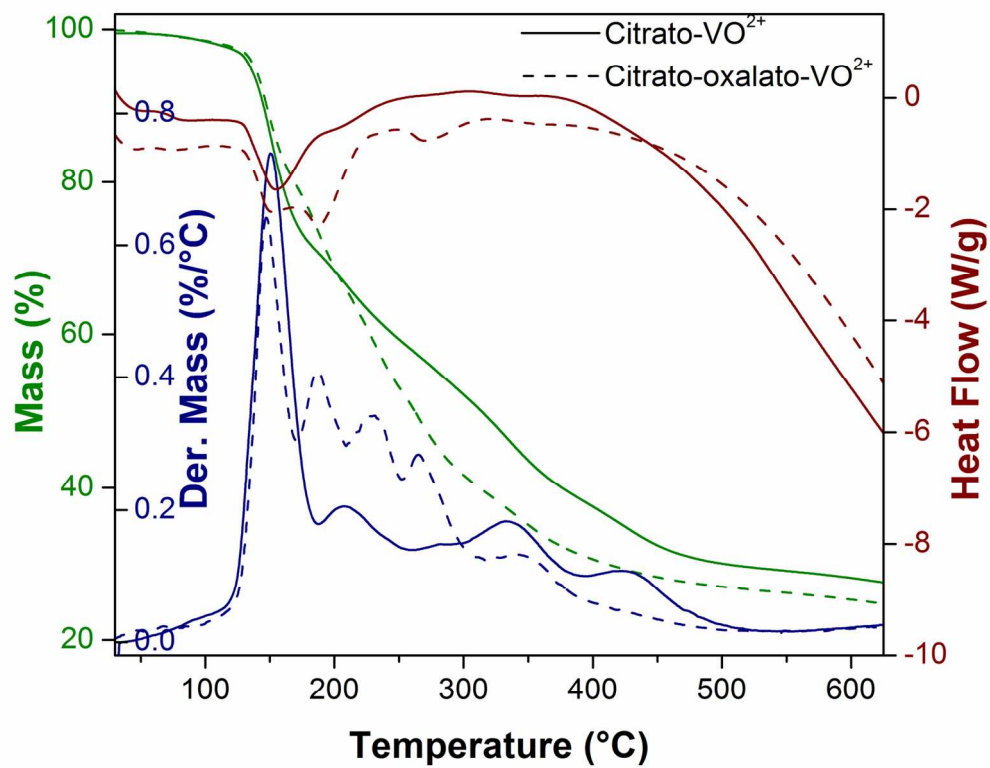


Figure 7: TGA (mass %), DTG (mass derivative) and DSC (heat flow) analyses of the citrato-oxalato-VO²⁺ and citrato-VO²⁺ precursor gel in N₂.
70x58mm (600 x 600 DPI)

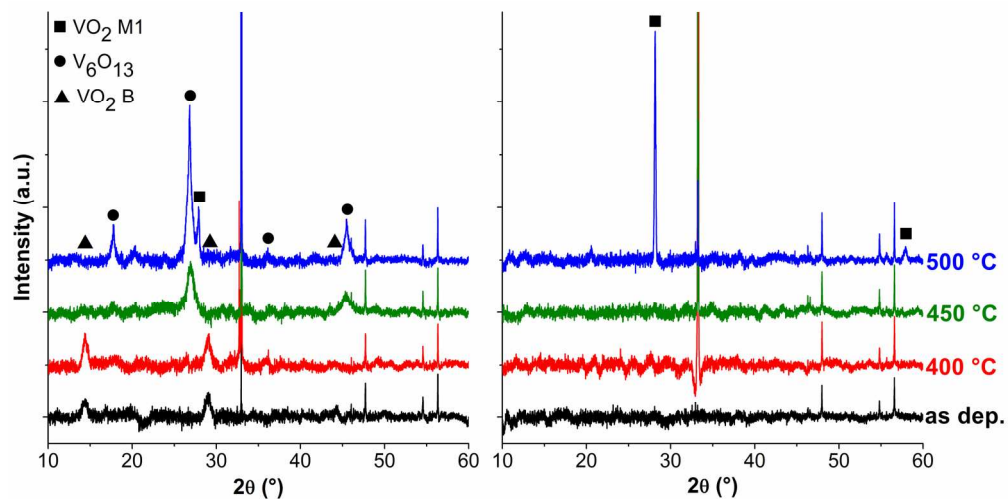


Figure 8: XRD pattern of 4 layered films spin coated from the aqueous citrato-oxalato- VO_2^{2+} (left) and citrato- VO_2^{2+} (right) precursor solution on 200 nm SiO_2 after an intermediate anneal of 400 °C (as deposited) and a post deposition anneal at 400 °C, 450 °C or 500 °C. All anneals are performed in a 0.1 % O_2 ambient for 10 minutes. The assignments are based on JCPDS 71-4821, 78-0983 and 81-2392 of, respectively, monoclinic VO_2 (M1), monoclinic V_6O_{13} and monoclinic VO_2 (B) (reference [50]).
84x42mm (600 x 600 DPI)

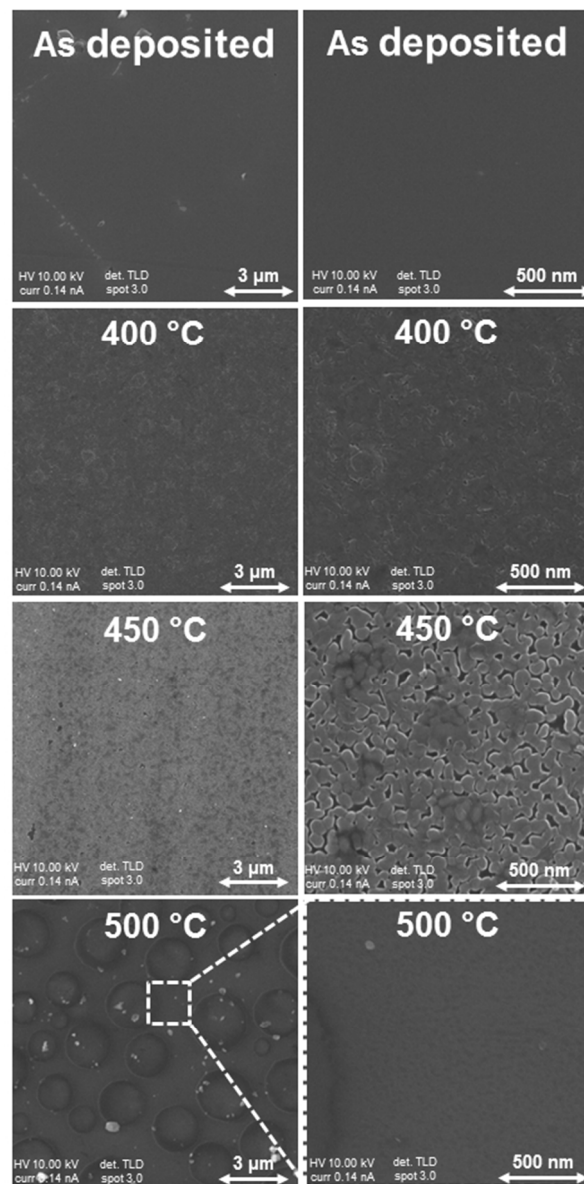
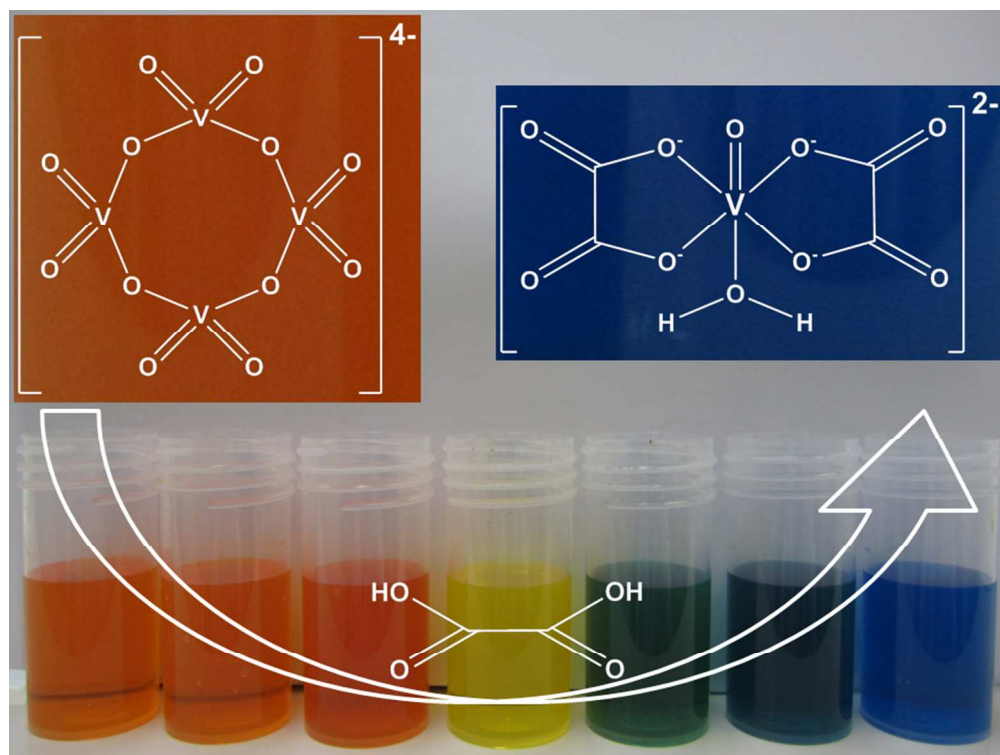


Figure 9: SEM images of 4 layered films spin coated from the aqueous citrato-VO²⁺ precursor solution on 200 nm SiO₂ after an intermediate anneal of 400 °C (as deposited) and a post deposition anneal at 400 °C, 450 °C or 500 °C. All anneals are performed in a 0.1 % O₂ ambient for 10 minutes.
127x254mm (96 x 96 DPI)



254x190mm (96 x 96 DPI)